pH-Titratable Superparamagnetic Iron Oxide for Improved Nanoparticle Accumulation in Acidic Tumor Microenvironments

Samuel H. Crayton and Andrew Tsourkas*

Department of Bioengineering, School of Engineering and Applied Science, University of Pennsylvania, Philadelphia, Pennsylvania 19104, United States

ABSTRACT

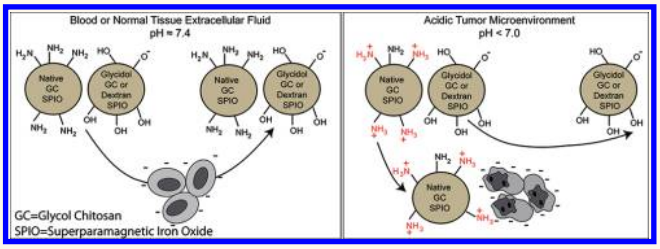

A wide variety of nanoparticle platforms are being developed for the diagnosis and treatment of malignancy. While many of these are passively targeted or rely on receptor–ligand interactions, metabolically directed nanoparticles provide a complementary approach. It is known that both primary and secondary events in tumorigenesis alter the metabolic profile of developing and metastatic cancers. One highly conserved metabolic phenotype is a state of up-regulated glycolysis and reduced use of oxidative phosphorylation, even when oxygen tension is not limiting. This metabolic shift, termed the Warburg effect, creates a "hostile" tumor microenvironment with increased levels of lactic acid and low extracellular pH. In order to exploit this phenomenon and improve the delivery of nanoparticle platforms to a wide variety of tumors, a pH-responsive iron oxide nanoparticle was designed. Specifically, glycol chitosan (GC), a water-soluble polymer with pH-titratable charge, was conjugated to the surface of superparamagnetic iron oxide nanoparticles (SPIO) to generate a T_2*-weighted MR contrast agent that responds to alterations in its surrounding pH. Compared to control nanoparticles that lack pH sensitivity, these GC-SPIO nanoparticles demonstrated potent pH-dependent cellular association and MR contrast *in vitro*. In murine tumor models, GC-SPIO also generated robust T_2*-weighted contrast, which correlated with increased delivery of the agent to the tumor site, measured quantitatively by inductively coupled plasma mass spectrometry. Importantly, the increased delivery of GC-SPIO nanoparticles cannot be solely attributed to the commonly observed enhanced permeability and retention effect since these nanoparticles have similar physical properties and blood circulation times as control agents.

KEYWORDS: glycol chitosan · Warburg effect · metabolic imaging · EPR · pH · SPIO

Tumor-targeting mechanisms that exploit the altered metabolic profile of malignancy have been the subject of intense investigation[1] since the development of the metabolite analogue 2-fluorodeoxy-D-glucose (2FDG) and its use in positron emission tomography (PET) imaging over three decades ago.[2] One of the attractions of metabolic imaging is the ability to detect and target a wide variety of cancers since many human solid tumors, and especially rapidly growing aggressive malignancies, have a unique metabolic profile that distinguishes them from normal tissue.[3] This altered metabolic state, consistent with the Warburg effect, is characterized by increased glucose uptake, up-regulated glycolytic metabolism, increased production of lactic acid, and subsequent derangements in cellular pH.[4,5] More specifically, the extracellular pH of normal tissue is approximately 7.4, but human and animal tumors can often exhibit an extracellular pH lower than 7.0, even reaching as low as 6.3.[6,7]

In recent years, numerous methods have been developed that allow for the noninvasive assessment of tissue pH, most of which are based on magnetic resonance.[6] For example, magnetic resonance spectroscopy (MRS) using endogenous inorganic phosphate (P_i) and exogenously administered 3-aminopropylphosphate (3-APP) can be used to simultaneously measure intra- and extracellular pH, respectively.[8,9] Major drawbacks of this method are the reliance on the relatively less abundant ^{31}P nucleus and the inability to simultaneously acquire the high-resolution anatomical information that is the hallmark of magnetic resonance (MR) imaging. More recently, exogenous agents with pH-dependent proton resonances have been developed.[10] While this eliminates the need for specialized ^{31}P hardware, the pH-sensitive resonance can be difficult to fully distinguish from other endogenous signals. Even more recently, pH-sensitive lanthanide chelates have allowed for measurement of pH with a proton resonance completely distinct from endogenous signals.[11,12] Even these agents, however, have limited sensitivity since the exogenous

* Address correspondence to atsourk@seas.upenn.edu.

Received for review July 28, 2011 and accepted October 29, 2011.

Published online October 29, 2011
10.1021/nn202863x

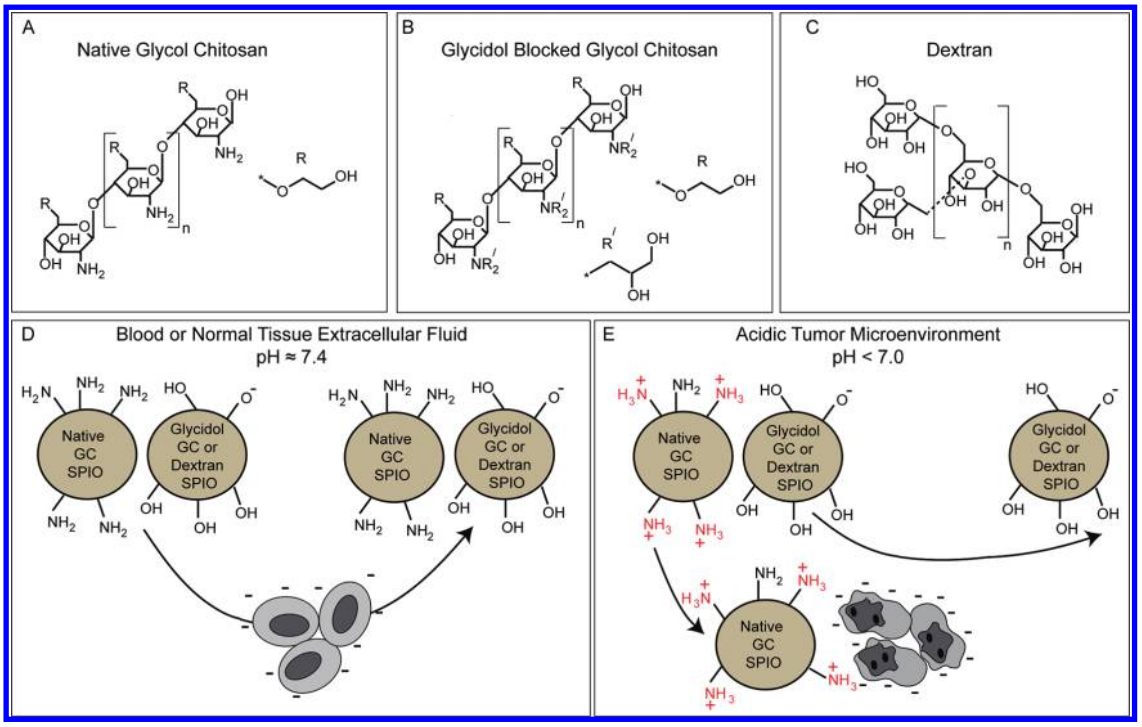

Figure 1. Schematic of pH-mediated enhanced delivery of native GC-SPIO nanoparticles in acidic microenvironments. (A) Native GC is a linear polymer of D-glucosamine with β-1−4 linkages. The repeated amino groups have aggregate p$K_a \approx 6.5$. (B) Glycidol blocked GC is formed by reaction of native GC with glycidol. Alkylation of the amino groups renders them no longer titratable near physiologic pH. (C) Dextran is a branched polymer of glucose with both α-1−3 and α-1−6 linkages. It does not possess any functional groups that are titratable near physiologic pH. (D) Both native GC-SPIO and control nanoparticles exhibit neutral to negative surface charge at physiologic pH due to abundant surface hydroxyl groups. For clarity, the hydroxyl groups are not depicted on the native GC-SPIO particle. Presence of neutral or negative surface charge diminishes nanoparticle association with blood components and normal tissue. (E) Upon exposure to acidic microenvironments, the amino groups of native GC-SPIO titrate to yield a positive charge. The newly cationic nanoparticles exhibit electrostatic interactions with negatively charged cell membranes and extracellular matrix components in the acidic microenvironment, leading to enhanced retention in these areas.

agent contains the resonance being detected. Greater sensitivity could be obtained using a contrast agent that generates signal by interacting with many bulk water molecules. Superparamagnetic iron oxide (SPIO) nanoparticles have emerged as an attractive class of MR contrast agent that provides T_2*-weighted contrast enhancement in both active and passive MR imaging applications by accelerating the dephasing of nearby bulk water.[13] SPIO nanoparticles could, therefore, serve as a strong signal-generating foundation to which pH sensitivity could be imparted. Such pH-responsive SPIO nanoparticles would constitute a ^{1}H MR contrast agent that exhibits differential localization based on local pH and could facilitate the detection of acidic pathologies, including but not limited to malignancy, on conventional high-resolution anatomic MR images, without the need for specialized hardware. Such regions of suspected acidity, detected with pH-responsive SPIO on large field-of-view anatomic images, could then be probed by MRS or chemical exchange saturation transfer (CEST) methods to generate an absolute pH map, if desired.

Several pH-responsive polymers, including chitosan,[14] polyamino ester,[15] polycaprolactone,[16] and polyhistidine,[17] have been successfully used to generate pH-mediated drug release in a variety of nanoparticle carriers. Furthermore, SPIO nanoclusters coated with a pH-responsive hydrogel have recently yielded nanoparticles with pH-dependent relaxivity.[18] Therefore, pH-titratable polymers have been used to impart unique functionality to nanoparticles in various contexts. In this investigation, the pH-responsive polymer glycol chitosan (GC, Figure 1A), a polymer of glucosamine with increased water solubility and amino groups with a p$K_a \approx 6.5$,[19] was covalently grafted to the surface of dextran-stabilized SPIO nanoparticles to generate native GC-SPIO. Sized matched pH-unresponsive SPIO nanoparticles were prepared as control agents to distinguish pH-mediated nanoparticle delivery from the enhanced permeability and retention (EPR) effect that is commonly observed for nanoparticle agents.[20−23] Specifically, GC-coated SPIO nanoparticles were chemically modified with glycidol (Figure 1B) to block the pH-responsive amino groups. In addition, inherently pH-unresponsive dextran SPIO nanoparticles (Figure 1C) were also used.

All nanoparticle formulations included a lanthanide metal tracer that allowed the distribution of the nanoparticles to be tracked quantitatively *in vivo*.

TABLE 1. Physicochemical Properties of Native GC-SPIO, Glycidol GC-SPIO, and Dextran SPIO Nanoparticles

particle surface	tracer lanthanide	mean hydrodynamic diameter (nm)	mean core size (nm)[a]	zeta (mV) at pH = 7.4	zeta (mV) at pH = 6.15	R_2 (mM^{-1} s^{-1})	R_1 (mM^{-1} s^{-1})
native GC	Gd	33.6	19.8 ± 3.6	+0.3	+8.2	146.5	7.5
glycidol GC	Gd	36.1	19.8 ± 3.6	−2.9	−1.0	152.3	7.9
dextran	Sm	29.8	19.4 ± 3.9	−20.4	−20.7	150.4	10.0

[a] Since the glycidol GC-SPIO was generated by direct surface modification of native GC-SPIO, core sizes for these formulations are identical.

Specifically, during the synthesis of the SPIO nanoparticles, a trace amount of lanthanide was doped into the iron oxide cores (Gd for the two GC-containing SPIO formulations and Sm for the dextran-only SPIO). The current authors have previously used energy-dispersive X-ray spectroscopy (EDS) to confirm the presence and stability of the lanthanide dopant within the iron oxide cores of SPIO synthesized in this manner (unpublished data). Here, inductively coupled plasma mass spectrometry (ICP-MS) was used to assess the biodistribution of the lanthanide tracer (and the corresponding SPIO nanoparticle) in a mouse tumor model.

Numerous studies have shown that nanoparticles (including SPIO) complexed with cationic agents such as polylysine, protamine, or cell-penetrating peptides (CPPs) are rapidly and efficiently internalized by a wide range of cell types.[24−27] However, positively charged nanoparticles are rapidly cleared from circulation,[28] resulting in poor tumor delivery. Therefore, positive charge could be used to improve retention in a desired microenvironment, provided that the positive charge is not displayed until that microenvironment is reached. Accordingly, both the native GC-SPIO and control agents exhibit a neutral or negative surface charge at physiologic pH, affording them a lower level of cellular interaction and improving blood residence time[29,30] (Figure 1D). Upon exposure to an acidic microenvironment, the pH-responsive polymer surface of the native GC-SPIO becomes protonated, and the surface charge becomes increasingly positive. Therefore, it was hypothesized that native GC-SPIO nanoparticles would be preferentially retained in acidic microenvironments compared with analogous pH-unresponsive agents, as a result of electrostatic interactions with surrounding tissue (Figure 1E).

RESULTS AND DISCUSSION

Characterization of Native GC-SPIO and Control Nanoparticles. Since previous studies have identified that the blood circulation times[20−23] and, consequently, tumor delivery, are highly dependent on the size of SPIO nanoparticles, the hydrodynamic diameter of the native GC-SPIO and control nanoparticles (*i.e.*, glycidol GC-SPIO, and dextran SPIO) was characterized by dynamic light scattering (DLS). Also, because of the need to distinguish pH-mediated delivery from a background level of EPR

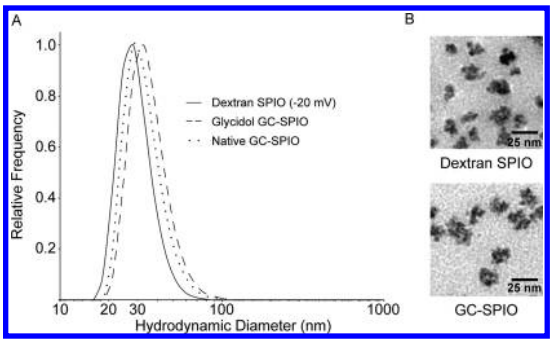

Figure 2. Size and morphology of native GC-SPIO, glycidol GC-SPIO, and dextran SPIO nanoparticles. (A) Dynamic light scattering profiles of each nanoparticle formulation in phosphate buffered saline, pH 7.4. (B) Transmission electron microscopy (TEM) images of GC-SPIO and dextran SPIO demonstrating iron core size and morphology.

delivery, it was necessary to ensure that the native GC-SPIO and control nanoparticles had very similar size profiles. The peak sizes of the native GC-SPIO, glycidol GC-SPIO, and dextran SPIO were found to be 33.6, 36.1, and 29.8 nm, respectively (Table 1). Since the glycidol GC-SPIO particles were synthesized by direct chemical blockade of the pH-sensitive amino groups of the native GC-SPIO, the glycidol GC-SPIO are necessarily slightly larger (2.5 nm). Although the size of dextran SPIO can be marginally tuned with varied synthetic conditions, these particles are necessarily slightly smaller (3.8 nm) than the native GC-SPIO, owing to the latter's additional GC coating. Given the close agreement in peak sizes and DLS size distributions (Figure 2A) for the three nanoparticle formulations, it is assumed that differences in tumor delivery can be attributed to differences in the chemistry of their surface coat, as opposed to their hydrodynamic diameter.

In order to examine the morphology of the iron cores of the nanoparticle formulations and ensure their similarity, transmission electron micrographs (TEM) were obtained (Figure 2B). The average core sizes of the GC-based SPIO and dextran SPIO were found to be 19.8 ± 3.6 and 19.4 ± 3.9 nm, respectively. Since only the surface coating was modified between the native GC-SPIO and glycidol GC-SPIO, these two formulations have matching core size characteristics. The morphology of iron cores appears similar for all three nanoparticle formulations and similar to previously published dextran SPIO images.[27]

The metal and polymer composition of the native GC-SPIO nanoparticles was further examined by elemental analysis. Dried nanoparticles were 37.05% C, 2.87% N, 6.09% Fe, and 0.17% Gd by weight. Since only GC contains nitrogen, these data and the known molecular structure of dextran and GC allow for calculation of nanoparticle composition. The native GC-SPIO nanoparticles are, therefore, 6.09% iron, 0.17% gadolinium, 39.08% dextran, and 42.02% glycol chitosan. The remainder of the nanoparticles (12.67%) is a combination of oxygen in the nanoparticle core and any electrostatically associated salts.

Although comparison of tumor delivery *via* ICP-MS measurements is not influenced by the nanoparticles' magnetic properties, the comparison of *in vivo* MR tumor contrast certainly is. Therefore, it was important to ensure that all three nanoparticle formulations had similar values for their relaxivities, especially the R_2 relaxivity, which is responsible for contrast enhancement on T_2*-weighted MR images. R_2 values (pH 7.4, PBS) for the native GC-SPIO, glycidol GC-SPIO, and dextran SPIO were measured as 146.5, 152.3, and 150.4 Fe mM^{-1} s^{-1}, respectively. The native GC-SPIO demonstrated only a minor increase in R_2 relaxivity (≈5%) as the pH decreased to 5.9, while the glycidol GC and dextran SPIO had no pH dependence in their R_2 values. Although improved relaxivity for the native GC-SPIO at low pH values can further improve pH-mediated contrast, the change in relaxivity was marginal and is not expected to be the primary mechanism by which contrast is generated. Further, given that the R_2 value for native GC-SPIO was slightly lower than the two control formulations at physiologic pH, it was concluded that there is no contrast bias for the native GC-SPIO.

Finally, the surface charge (zeta-potential), and its pH dependence, was examined for each of the nanoparticle formulations (Figure 3). The native GC-SPIO nanoparticle was found to have a near-neutral zeta-potential (+0.3 mV) at physiologic pH = 7.4. It is important for tumor delivery that the native GC-SPIO have little or no positive surface charge at normal blood pH because cationic materials are rapidly cleared from circulation, due to local electrostatic interactions, before they could reach a tumor.[28] Next, as the pH was lowered, the zeta-potential continually increased and reached a value of +4.1 mV at pH = 6.65 and +8.2 mV at pH = 6.15. Therefore, it was confirmed that the native GC-SPIO nanoparticles had a surface coat capable of meaningfully sensing a pH drop of 1.0 unit or less. Since a wide variety of cationic materials have been found to electrostatically associate with cells,[24−27] it was expected that the surface properties of the native GC-SPIO nanoparticles would allow them to adhere to cells or negatively charged extracellular matrix components in a pH-dependent manner that is favorable for detection of acidic environments.

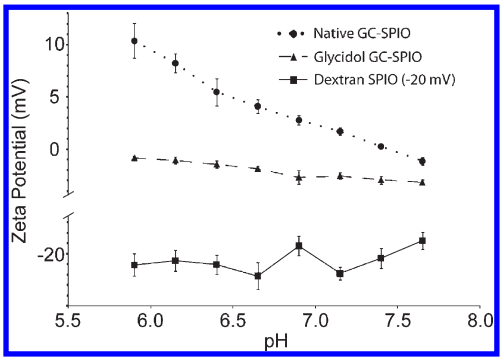

Figure 3. Zeta-potential (surface charge) titration of native GC-SPIO, glycidol GC-SPIO, and dextran SPIO nanoparticles at 100 μg/mL nanoparticle concentration in 10 mM HEPES buffer at various pH.

The pH dependence of the surface charge was similarly investigated for the glycidol GC-SPIO and dextran SPIO nanoparticles. At physiologic pH = 7.4, the zeta-potentials were −2.9 and −20.4 mV for the glycidol GC-SPIO and dextran SPIO, respectively. Upon lowering of the pH to 6.15, the zeta-potentials changed to −1.0 and −20.7 mV. These results indicate that the surface charge of the control nanoparticles does not have significant pH dependence; under conditions that lead to an increase in the zeta-potential of the native GC-SPIO by 7.9 mV, the glycidol GC-SPIO increased only 1.9 mV, and the dextran SPIO zeta-potential dropped by 0.3 mV (a difference within the standard deviation of a given measurement). It should be noted that the zeta-potential of both control nanoparticles remains below 0 mV under every pH condition, such that not even an extremely acidic tumor environment would be able to induce electrostatic adherence of these nanoparticles.

It should also be noted that the two GC-based nanoparticle formulations have close to neutral and very similar surface charge at physiologic pH = 7.4. In fact, their surface charges proved similar enough to give them overlapping blood circulation profiles (see below). The glycidol GC-SPIO control formulation, therefore, specifically isolates the EPR component of tumor delivery from the neutrally charged native GC-SPIO formulation, so that pH-mediated improvement can be assessed. Additionally, since previous investigation of nanoparticle blood clearance has shown that prolonged circulation times may be achieved with neutral or negative formulations,[29,30] the −20 mV dextran formulation was included as a second control to assess tumor delivery for a nontitratable nanoparticle with negative charge.

***In Vitro* pH-Dependent Association of Native GC-SPIO.** Following the successful synthesis of the native GC-SPIO, possessing a favorably pH-dependent surface charge, as well as size and relaxivity matched pH-independent control nanoparticles, the ability of each formulation to label tumor cells *in vitro* and generate *in vitro* MR

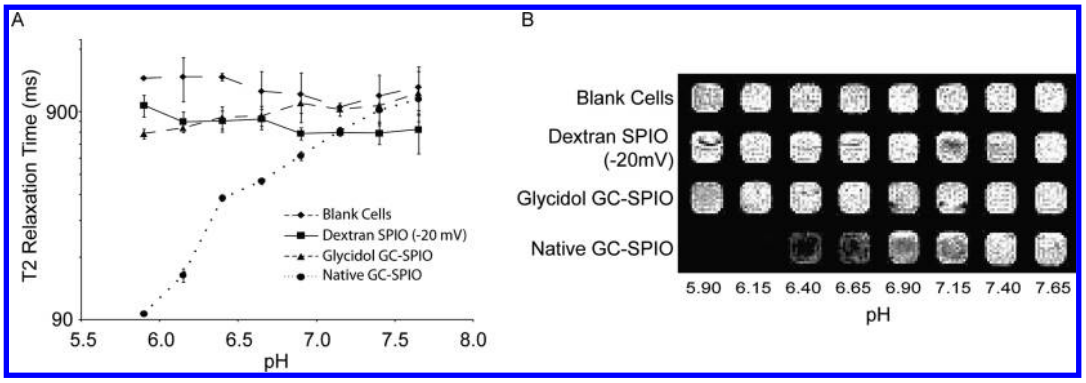

Figure 4. ***In vitro*** **association of native GC-SPIO, glycidol GC-SPIO, and dextran SPIO nanoparticles with T6−17 cells. (A) Nanoparticles were incubated in triplicate at 25 μg Fe/mL with 4 $\times$ 10^6 T6−17 cells in culture medium buffered by 25 mM HEPES. After removal of unassociated nanoparticles, T_2 relaxation times were collected for each cellular suspension. (B) Triplicate samples at each pH were combined into a single cell pellet, and a T_2*-weighted MR image was obtained. Pellets with low T_2 relaxation times, resulting from the presence of nanoparticles, appear with reduced signal intensity in the image.**

contrast was investigated under various pH conditions. Specifically, each nanoparticle formulation was incubated in triplicate with T6−17 tumor cells in culture medium at a concentration of 25 μg Fe/mL at pH values ranging from 5.9 to 7.65, in 0.25 unit increments. Following triplicate washing to remove unassociated nanoparticles, the T_2 relaxation times of the cell suspensions were measured to access the extent of cell association (Figure 4A).

Interestingly, it was found that cells incubated with native GC-SPIO nanoparticles exhibited a pronounced pH dependence in their T_2 relaxation times. At physiologic pH = 7.4, the native GC-SPIO cells had an average T_2 relaxation time of 917 ms that was not statistically different from the T_2 relaxation times of cells incubated with either control nanoparticle or blank cells incubated without nanoparticles. However, when the pH was dropped only one-quarter of a pH unit to 7.15, the average T_2 relaxation time of native GC-SPIO incubated cells dropped to 728 ms. Although not a particularly robust T_2 value, 728 ms was statistically different from the values of 950 and 927 ms observed for cells incubated without nanoparticles or glycidol GC-SPIO control nanoparticles, respectively. These results suggest that, under ideal conditions, the pH-titratable native GC-SPIO nanoparticles can differentially label cells in microenvironments only 0.25 pH units below physiologic value. After another 0.25 unit drop in pH to 6.90, the native GC-SPIO nanoparticle incubated cells obtained an average T_2 value of 553 ms, which was statistically different from blank cells and cells incubated with both control nanoparticle formulations. With further reductions in the incubation pH, the average T_2 value for cells incubated with native GC-SPIO continued to decrease, ultimately reaching values of 147 ms at pH 6.15 and 96 ms at pH 5.90.

Appropriately, neither the glycidol GC nor dextran SPIO control nanoparticles exhibited any meaningful pH dependence in their cellular association. Although the glycidol GC-SPIO cells incubated at very low pH values (5.90 and 6.15) yielded T_2 relaxation times that were statistically different from the value at physiologic pH = 7.4, the T_2 values at low pH were still greater than 700 ms, indicating a weak signal. Recall that native GC-SPIO incubated cells had already reached this relaxation level at pH 7.15. The statistically detectable difference in relaxation for the glycidol GC-SPIO incubated cells at the two extremes of pH is likely due to a small population of titratable amino groups remaining despite chemical blockade. For the dextran SPIO, there was no statistically detectable difference in cell association between the two ends of the pH spectrum.

It is also noteworthy that native GC-SPIO nanoparticles are able to produce T_2 relaxation times under 200 ms in these cell pellet studies at concentrations of only 25 μg Fe/mL. For comparison, actively targeted SPIO nanoparticles relying on receptor−ligand interactions have been tested under similar conditions and yielded similar T_2 relaxation times when incubated at concentrations of 150 μg Fe/mL.[31] Although such a comparison is not exact, these results indicate that native GC-SPIO nanoparticles may be able to generate contrast of a magnitude similar to receptor-targeted SPIO nanoparticles.

Following measurement of their T_2 relaxation times, the cell pellets were transferred to a well plate and a T_2*-weighted MR image was acquired (Figure 4B). For the cells incubated with native GC-SPIO, signal loss can already be discerned at a pH of 7.15, only 0.25 units below physiologic pH. The signal loss becomes more pronounced as the incubation pH drops to 6.65, and at pH 6.15 and below, the signal is lost entirely under these imaging parameters. Importantly, the cells incubated with glycidol GC and dextran SPIO control nanoparticles do not exhibit any marked pH dependence in their MR signal intensity.

In Vivo **MR Contrast Enhancement of Native GC-SPIO.** The ability of native GC-SPIO to generate MR contrast significantly greater than the background EPR effect was confirmed with an *in vivo* murine tumor model.

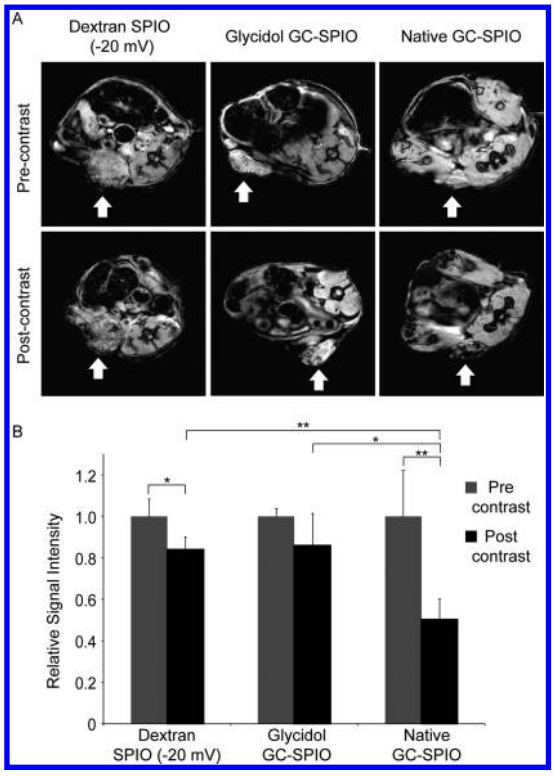

Figure 5. ***In vivo*** **MR images and intensity analysis of nu/nu nude mice with T6−17 flank tumors. (A) Representative T_2*-weighted MR images in the axial plane prior to injection (precontrast) and 24 h after injection (postcontrast) of native GC-SPIO ($n = 4$), glycidol GC-SPIO ($n = 4$), and dextran SPIO ($n = 3$) nanoparticles. Tumor location is indicated by white arrows. (B) Quantitative analysis of MR images. Signal intensity of each tumor was normalized to adjacent paraspinal muscle. For contrast measurement, the relative signal intensity, RSI, was calculated as the quotient of the postcontrast to precontrast normalized tumor intensity. For *t* test statistical analysis of the groups, statistically significant values of $p < 0.05$ are indicated with single asterisk and $p < 0.005$ with double asterisk.**

Specifically, T6−17 flank tumors were grown in nude mice to a diameter of approximately 8 mm, and then either native GC-SPIO or control nanoparticles at a dose of 10 mg Fe/kg body weight (approximately 0.2 mg of iron per animal) was administered intravenously. T_2*-weighted MR images were acquired immediately prior to injection of nanoparticles and 24 h after injection (Figure 5). The postcontrast images of the native GC-SPIO nanoparticle demonstrated striking relative signal loss in the tumor. In the precontrast image shown, the tumor is located between iso-intense paraspinal and thigh muscles and is not clearly delineated. In the postcontrast image, however, the tumor is revealed as a hypo-intense heterogeneous region, with well-defined margins, exerting a mass effect against the adjacent paraspinal muscle. The heterogeneity of intensity within the tumor is likely caused by impaired SPIO diffusion and penetration once they encounter a microregion of sufficient acidity, either at the negatively charged tumor vascular endothelium or within the tumor interstitium. Alternatively, the heterogeneity may reflect variations in extracellular pH within the tumor.[32] Neither the glycidol GC nor dextran SPIO control nanoparticles yielded significantly visible contrast enhancement between pre- and postcontrast images.

The MR signal in the tumor regions of interest (ROIs) was also analyzed quantitatively (Figure 5B). For each animal, three matching axial slices were examined pre- and postcontrast. Variations in absolute signal from slice to slice, due to mouse or RF coil positioning, were accounted for by normalizing the tumor signal to that of adjacent paraspinal muscle on a slice by slice basis. The native GC-SPIO nanoparticles yielded a contrast enhancement (relative signal intensity ratio) of 0.50. In this scale, lower values indicate greater contrast, with 1.0 corresponding to no contrast and 0 indicating perfect contrast. Importantly, the contrast enhancement observed for native GC-SPIO nanoparticles was statistically different from that of glycidol GC and dextran SPIO, which had RSI ratios of 0.86 and 0.84, respectively.

Interestingly, the RSI ratio obtained for these native GC-SPIO nanoparticles was comparable to that obtained in a study of actively targeted SPIO nanoparticles injected at the same concentration and directed against the same tumor cell line.[31] While many variables influence the contrast enhancement observed *in vivo*, it is encouraging to see that the pH-titratable native GC-SPIO nanoparticles can deliver contrast enhancement on the same order as actively targeted agents.

In Vivo **Tumor Delivery and Blood Clearance.** To specifically examine the amount of nanoparticle delivery to the tumor, as well as investigate blood circulation profiles, the nanoparticle formulations were designed with unique lanthanide metal tracers that can be detected by ICP-MS. Immediately after the postcontrast images were acquired, each animal was sacrificed and the flank tumors were removed. By comparing the amount of lanthanide tracer present in the excised tumors to the amount of lanthanide present in the original intravenous injection, the amount of nanoparticle delivery can be quantified as a percent of injected dose per gram of tumor tissue (Figure 6A). Also, these data can be converted into absolute iron concentrations since the amount of injected material is known. The nanoparticle iron concentrations in the tumor were thus calculated as 2.5, 4.2, and 6.7 μg/mL for dextran, glycidol, and native GC-SPIO, respectively.

Interestingly, even though MR imaging yielded similar contrast enhancement for the glycidol GC-SPIO and dextran SPIO, there was significantly more nanoparticle delivery for the glycidol GC-SPIO. The contrast enhancement observed in MR images reflects the combination of many variables, including, but not limited to, concentration of agent in the tumor, MR pulse sequence parameters (*e.g.*, TE), and nanoparticle

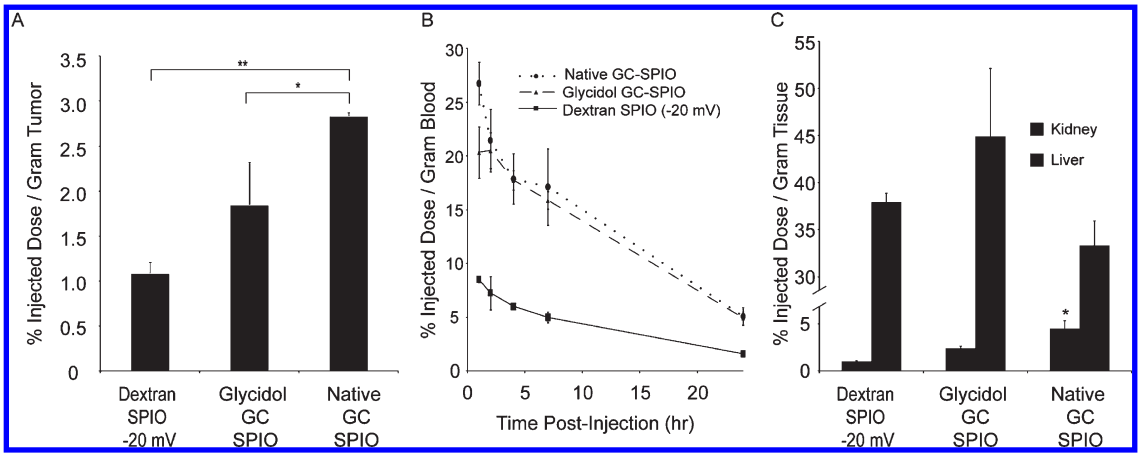

Figure 6. Quantitative tumor delivery, blood clearance, and other organ concentrations of native GC-SPIO, glycidol GC-SPIO, and dextran SPIO. (A) Percent injected dose per gram of tumor tissue was calculated by measuring the concentration of lanthanide tracer in excised tumors using ICP-MS. For the native GC-SPIO, this converts to approximately 6.7 μg Fe/mL. For *t* test statistical analysis of the groups, statistically significant values of $p < 0.05$ are indicated with single asterisk and $p < 0.005$ with double asterisk. (B) Nanoparticle blood clearance as measured by concentration of lanthanide tracer in the blood. (C) Kidney and liver concentrations of native GC-SPIO and control nanoparticles 24 h postinjection. Asterisk indicates statistical significance ($p < 0.05$) between native GC-SPIO kidney uptake and either control nanoparticle.

relaxation characteristics (*e.g.*, R_2). Specifically, the nanoparticles have a dynamic concentration range in which they linearly decrease the tissue's relaxation time. For the SPIO used in this study, the dynamic range, determined during *in vitro* relaxation measurements, was 1−50 μg/mL (at 1.4 T). Little contrast may be observed with nanoparticle concentrations at the low end of this range; significant improvements in contrast occur near the middle of the range, and saturation occurs at the top. It is likely that the nanoparticle concentrations achieved by dextran and glycidol GC-SPIO are very near the bottom of the dynamic range, still not high enough to generate significant contrast with the pulse sequence parameters used.

The animals injected with native GC-SPIO nanoparticles showed a further significant increase in tumor delivery from the glycidol GC-SPIO. Importantly, this pH-mediated increase in nanoparticle delivery was sufficient to reach a concentration providing much more MR contrast. This demonstrates the importance of optimizing and maximizing nanoparticle delivery since the incremental improvement in delivery (*i.e.*, from glycidol GC-SPIO to native GC-SPIO) has the possibility to yield significant contrast improvement. It is envisioned that, while a completely passive agent might not reach a concentration detectable on an MR image, the additional improvement in delivery obtained by a pH-sensitive agent could result in detectable MR contrast.

It has been well-established that entirely passive tumor delivery of nanoparticles *via* EPR is a function of the pharmacodynamics of their blood circulation.[20−23] The two GC-based formulations are of similar size, have a similar (although not exactly identical) zeta-potential at the physiologic pH of 7.4, and have a surface coat constructed from the same polymer. These two formulations, therefore, were expected to have very similar blood circulation profiles. This important hypothesis was validated by using ICP-MS to measure the blood concentration for each nanoparticle as a function of time (Figure 6B). As anticipated, the native GC-SPIO and glycidol GC-SPIO were found to have very well overlapped blood circulation profiles. Importantly, the small difference between the native GC-SPIO and glycidol GC-SPIO surface charge at physiologic pH did not alter their blood clearance. Therefore, it can be concluded that the incremental improvement in delivery that native GC-SPIO exhibits over glycidol GC-SPIO represents pH-mediated delivery, not attributable to EPR.

In order to see how the pH-enhanced tumor delivery of native GC-SPIO compares to the EPR that could be obtained with a negative instead of neutral surface charge, it is helpful to examine the tumor delivery and blood clearance of the dextran SPIO nanoparticles at −20 mV. It was found that the negatively charged dextran accumulated in the tumor at lower levels (Figure 6A) than the native GC-SPIO or the neutrally charged glycidol GC-SPIO. The lower accumulation observed for the −20 mV dextran correlated with its shorter blood residence time (Figure 6B), which is characteristic of passive delivery by EPR. Furthermore, in a complementary study examining the effect of surface charge on passive tumor delivery, the authors evaluated dextran SPIO with pH-independent zeta-potentials of approximately −12, −5, +4, +10, and +14 mV (unpublished data). Like the −20 mV dextran SPIO nanoparticles in this study, none of the pH-insensitive dextran SPIO nanoparticles accumulated as well as native GC-SPIO (*i.e.*, statistically significant inferior delivery for every dextran SPIO nanoparticle). In fact, the dextran SPIO with strongly positive surface charge accumulated especially poorly at the tumor site.

It is, therefore, important for the mechanism of native GC-SPIO delivery that the nanoparticles not constitutively display a large positive surface charge—rather only after entering the tumor microenvironment.

Finally, in addition to the pathological environment of a tumor, other groups investigating pH-responsive agents have demonstrated that there are physiologically normal sites of pH <7.4, such as the renal tubular system.[33−35] Therefore, the delivery of native GC and control SPIO nanoparticles to the kidneys was examined. At 24 h postinjection, the average renal concentrations, expressed as percent of injected dose per gram of kidney tissue, were found to be 4.49, 2.40, and 1.02 for native GC-SPIO, glycidol GC-SPIO, and dextran SPIO (−20 mV), respectively (Figure 6C). Given the longer blood residence times for the two GC-based formulations, it is not surprising to observe a greater renal concentration at 24 h for those formulations compared to the dextran SPIO. Interestingly, though, the renal concentration of the native GC-SPIO was a statistically significant 87% higher than that of the glycidol GC-SPIO, despite very similar blood circulation profiles and identical blood concentrations at the 24 h time point. Furthermore, the native GC-SPIO nanoparticles are not simply being deposited to a higher extent in all organs since the concentrations of all three nanoparticles in the liver at 24 h were not statistically distinct from one another. Despite the lack of statistical significance, the native GC SPIO nanoparticles had a trend toward *less* accumulation in the liver (33.3 *versus* 44.9 and 37.9 for the glycidol GC and dextran SPIO, respectively, Figure 6C).

CONCLUSION

The biocompatible and biodegradable polymer glycol chitosan can be used to impart pH-responsiveness to superparamagnetic iron oxide nanoparticles. The resulting material demonstrates a pH-dependent surface charge, allowing it to achieve long blood circulation at physiologic pH = 7.4 and then transition to a cationic and adhesive form upon entering an acidic microenvironment at pH <7.0. These native GC-SPIO nanoparticles exhibited significantly improved accumulation in a murine tumor model, compared to nanoparticles with similar physical properties, but lacking pH-responsiveness. Higher levels of SPIO accumulation in the tumor also resulted in a clear and quantifiable improvement in magnetic resonance contrast, as shown on T_2*-weighted images. Generally, it is believed that glycol chitosan could be used to exploit the metabolic profile of a wide range of malignancies and improve the tumor delivery of imaging or therapeutic agents, provided that synthesis of such agents preserves the pH-responsive amino group.

METHODS

Synthesis of Dextran-Stabilized Lanthanide-Doped SPIO. Dextran-coated, lanthanide-doped SPIO nanoparticles were prepared through the co-precipitation of ferrous, ferric, and lanthanide ions in the presence of dextran.[27] Briefly, 50 g of dextran T-10 (Pharmacosmos A/S, Holbaek, Denmark) was dissolved in 100 mL of dH_2O and heated to 80 °C for 1 h. The solution was then allowed to cool to room temperature and continued to mix overnight. Subsequently, a solution of 3.70 g of $FeCl_3$, 1.46 g of $FeCl_2$, and 0.25 g of $GdCl_3 \cdot 6H_2O$ or $SmCl_3 \cdot 6H_2O$ in 50 mL of dH_2O was prepared and decanted into the dextran solution. The combined solution was cooled on ice and degassed with N_2 for 90 min. While keeping the solution stirring on ice and under N_2, an automated syringe pump was then used to introduce 15 mL of concentrated NH_4OH to the solution over 5 h. The resulting black viscous solution was removed from the N_2 atmosphere, heated to 90 °C for 1 h, cooled overnight, and centrifuged at 20 000 rcf for 30 min to remove large aggregates. Free iron, lanthanide, and dextran were removed by diafiltration across a 100 kDa membrane, and the dextran SPIO was brought to a final volume of 40 mL.

Surface Conjugation of Glycol Chitosan. High molecular weight glycol chitosan (Wako Chemicals, Richmond, VA, USA) was degraded and prepared for grafting to dextran SPIO as follows: 10 g of ≈600 kDa GC was dissolved in 200 mL of 6 M HCl and heated to 80 °C for 20 min. Following incubation, the material was cooled on ice and immediately neutralized with the addition of solid sodium carbonate to terminate degradation. Excess solid sodium carbonate was removed by centrifugation, and diafiltration membranes were used to desalt the material and discard any GC polymer greater than 100 kDa or less than 3 kDa.

Native glycol chitosan (GC)-SPIO was then prepared as follows: 40 mL of dextran SPIO at an iron concentration of 10 mg/mL was combined with an equal volume of 10 M NaOH and mixed for 10 min. Then, 80 mL of epichlorohydrin was added, and the solution was vigorously stirred at room temperature overnight. Epichlorohydrin cross-links dextran chains within a SPIO particle and chemically activates the dextran surface for grafting of glycol chitosan. The solution was then briefly centrifuged to allow phase separation into an aqueous black SPIO layer and a clear layer of unreacted epichlorohydrin, which was removed. The SPIO layer was quickly purified *via* extraction in isopropyl alcohol. Specifically, the SPIO material was combined with 5 volumes of isopropyl alcohol, and the mixture was vigorously shaken. Brief centrifugation of the mixture resulted in a layer of precipitated salt, a SPIO layer, and an isopropyl alcohol layer (containing any remaining epichlorohydrin). The SPIO layer was then isolated and combined with an equal volume of 150 mg/mL GC (3−100 kDa) in PBS and gently stirred for 72 h at room temperature. After the reaction, free GC was removed by diafiltration across a 100 kDa membrane, and the final native GC-SPIO was 0.2 μm filtered to remove any oversized material. Finally, to ensure complete purification of the GC-SPIO from excess GC and to enhance the material's magnetic properties, the nanoparticles were magnetically purified on MACS LS columns using the MidiMACS magnet (Miltenyi Biotec, Auburn, CA, USA).

Generation of Control SPIO Nanoparticles. Glycidol GC-SPIO control nanoparticles were produced by direct chemical modification of the native GC-SPIO nanoparticle surface. Briefly, native GC-SPIO at 5 mg of Fe/mL in 10 mM pH 5.0 HEPES buffer was combined with an equal volume of glycidol and stirred at room temperature overnight. GC-SPIO was then precipitated from the solution by the addition of 4 volumes of isopropyl alcohol. Since the blocking was incomplete after only one round of reaction with glycidol, the addition at 0.2 volumes of 7.5% sodium bicarbonate was sometimes required to neutralize remaining positive charge on the nanoparticle surface and induce

precipitation. The solution was centrifuged, the supernatant discarded, and the GC-SPIO pellet resuspended with sonication in the original volume of HEPES buffer. Reaction with glycidol was repeated as above two more times to exhaustively block pH-responsive amino groups (subsequent reactions do not require bicarbonate to induce precipitation in isopropyl alcohol). Finally, size-matched dextran SPIO was used as a second pH-unresponsive control nanoparticle formulation. In order to best match the size of the dextran SPIO control nanoparticles to the GC-grafted nanoparticles, the dextran SPIO nanoparticles used as a control were not from the same synthesis as the dextran SPIO upon which the GC-grafted nanoparticles were constructed. Specifically, the rate of NH_4OH addition was increased in order to produce somewhat larger-sized dextran SPIO.

Native GC-SPIO and Control Nanoparticle Physicochemical Characterization. Each nanoparticle formulation was diluted to a final concentration of 100 μg Fe/mL in pH 7.4 phosphate buffered saline for determination of the hydrodynamic diameter by dynamic light scattering (DLS). Measurements were acquired with a Zetasizer Nano-ZS (Malvern Instruments, Worcestershire, UK) using the non-invasive backscatter (NIBS) mode. Samples were further diluted in water and deposited on 200-mesh carbon-coated copper grids (Polysciences, Warrington, PA, USA) for TEM imaging with a JEOL 1010 transmission electron microscope operating at 80 kV. Mean iron core size was determined by measuring 100 individual nanoparticles. The transverse (R_2) and longitudinal (R_1) relaxivities of the nanoparticle formulations were calculated by plotting the reciprocal of the relaxation time (measured using a Bruker mq60 tabletop MR relaxometer operating at 1.41 T) *versus* the iron concentration. For elemental analysis, nanoparticles were precipitated with isopropyl alcohol, dried under vacuum, and submitted to Intertek Analytical Laboratories (Whitehouse, NJ, USA). Since glycol chitosan is the only nitrogen-containing component of the nanoparticles, the %N of the sample can be scaled to %GC, using the empirical formula of glycol chitosan, $C_8H_{15}O_5N$. Similarly, since dextran is the only carbon-containing component (after the carbon content of GC is accounted for), the %dextran can be calculated using its empirical formula, $C_6H_{10}O_5$. For zeta-potential pH titrations, 10 mM HEPES buffered water was prepared with pH values ranging from 5.90 to 7.65 in 0.25 unit increments. Each nanoparticle formulation was diluted to a final concentration of 100 μg Fe/mL in the buffer at each pH, and mean nanoparticle zeta-potential was measured using a Zetasizer Nano-ZS. Stocks of native GC-SPIO, glycidol GC-SPIO, and dextran SPIO were synthesized several times throughout the course of the study, each time yielding similar physicochemical properties.

Cell Culture. T6−17 murine fibroblasts (a derivative of the NIH/3T3 line and kindly provided by Mark Greene, Ph.D., FRCP, University of Pennsylvania) were cultured and maintained in Dulbecco's modified Eagle's medium (DMEM), supplemented with 10% fetal bovine serum (FBS), 1% penicillin/streptomycin at 37 °C and 5% CO_2.

***In Vitro* Cellular Association Studies.** For *in vitro* pH studies, cell culture medium was supplemented with 25 mM HEPES buffer and prepared with pH values ranging from 5.90 to 7.65 in 0.25 unit increments. Each nanoparticle formulation was incubated in suspension at a concentration of 25 μg Fe/mL with 4×10^6 of freshly trypsinized T6−17 cells for 1 h at 37 °C in a total volume of 0.5 mL buffered medium. Following incubation, unassociated nanoparticles were removed by triplicate low-speed centrifugal washes with nanoparticle-free medium of matching pH. The cell samples were then resuspended in 0.3 mL of PBS at pH 7.4, and the T_2 relaxation times of the suspensions were measured on the tabletop relaxometer.

Cell Pellet MR Imaging. Following relaxation measurements, the triplicate samples at each pH were combined to form a single cell pellet for each pH and nanoparticle formulation. The samples were transferred to a 384-well plate, and the cells were pelleted to the bottom of each well with brief, low-speed centrifugation. The plate was then imaged on a 9.4 T magnet interfaced to a Varian INOVA console using a 70 mm inner diameter volume coil for radio-frequency transmission and reception. T_2*-weighted gradient echo (GEMS) MR images were collected using parameters as follows: repetition time (TR) = 200 ms, echo time (TE) = 5 ms, flip angle = 20°, slice thickness = 0.5 mm, field of view (FOV) = 4 cm × 4 cm, number of acquisitions = 8, resolution = 256 × 256.

Contrast Enhanced *In Vivo* MR Imaging. Approximately 6 week old female nu/nu nude mice (Charles River Laboratory, Charles River, MS, USA) were maintained in accordance with the Institutional Animal Care and Use Committee of the University of Pennsylvania. Mice were anesthetized *via* isoflurane, and T6−17 cells were injected subcutaneously into the back right flank (2×10^6 cells in 0.2 mL of PBS). Tumors were grown until the diameter was approximately 8 mm, and precontrast tumor images were acquired using a 9.4 T magnet interfaced to a Varian INOVA console. T_2*-weighted GEMS images were collected using the same parameters as for plate images, except slice thickness = 1 mm. Immediately following the precontrast image acquisition, native GC-SPIO or control nanoparticles were administered by retro-orbital injection (10 mg/kg Fe in 0.2 mL; native GC-SPIO $n = 4$, glycidol GC-SPIO $n = 4$, dextran SPIO $n = 3$). Postcontrast images were collected 24 h postinjection under the same imaging parameters used for precontrast images.

MR Image Analysis. For each animal's pre- and postcontrast image, three corresponding axial slices were selected for analysis. To account for signal variations between images due to mouse or RF coil positioning, the relative signal intensity (RSI) of the tumor in each slice was calculated by dividing the MR signal of the operator defined tumor region of interest (ROI) by that of the adjacent paraspinal muscle. Nanoparticle-induced tumor contrast was then determined as the RSI ratio for each animal, calculated as the quotient of the postcontrast tumor RSI to the precontrast tumor RSI. Following statistically significant ANOVA analysis for the three nanoparticles' contrast, individual *t* tests were performed.

Quantitation of Tumor Delivery and Blood Concentration by ICP-MS. Prior to nanoparticle injection, an aliquot of nanoparticles from each group of mice was saved for inductively coupled plasma mass spectrometry (ICP-MS) determination of lanthanide concentration (Gd for native and glycidol GC-SPIO and Sm for dextran SPIO). Following nanoparticle injection, 10 μL blood samples were collected from each animal, using the tail-nick method, at times of 1, 2, 4, 7, and 24 h postinjection. Following postcontrast MR imaging, the animals were sacrificed and the tumors, livers, and kidneys excised.

For ICP-MS analysis, analytical standards were purchased from SCP (Champlain, NY, USA) and trace metal grade nitric acid was purchased from Fisher Scientific (Pittsburgh, PA, USA). All dilutions were done using in-house deionized water (≥18 MΩ·cm) obtained from a Millipore water purification system.

The preinjection solutions, blood, and tumor samples were analyzed for ^{158}Gd (gadolinium) or ^{147}Sm (samarium) using an Elan 6100 ICP-MS (Perkin-Elmer, Shelton, CT, USA) at the New Bolton Center Toxicology Laboratory, University of Pennsylvania, School of Veterinary Medicine, Kennett Square, PA, USA. The samples were weighed into Teflon PFA vials (Savillex, Minnetonka, MN, USA) and digested overnight with 70% nitric acid at 70 °C. Then, 0.1 mL of 2 ppm ^{159}Tb (terbium) was added to each of the digested samples, and the mixtures were diluted with deionized water to a final volume of 10 mL. The lanthanide concentration of each sample was measured using a calibration curve of aqueous standards at 0.01, 0.1, 1.0, and 10 ppb for each lanthanide.

The performance of the instrument and accuracy of the results were monitored by analyzing a reagent blank and bovine serum control serum (Sigma) prior to analysis of the samples. Also, standard reference material (Peach Leaves 1547) obtained from National Institute of Standards and Technology (NIST, Gaithersburg, MD, USA) with known values of iron and rare earth elements was analyzed with each batch of samples.

The percent injected dose per gram of tissue was calculated as $[Ln]_{sample}/([Ln]_{inj} \times M_{inj})$, where $[Ln]_{sample}$ is the lanthanide concentration in the sample (blood or tumor tissue), $[Ln]_{inj}$ is the lanthanide concentration in the injected nanoparticle solution, and M_{inj} is the mass of nanoparticle solution injected (0.2 g). For tumor, kidney, and liver accumulation, ANOVA analysis was performed for the three nanoparticle formulations. Where differences were detected (tumor and kidney), individual *t* tests were performed.

Acknowledgment. This work was supported in part by the National Institutes of Health (NCI) R21 CA140695 and the Department of Defense Breast Cancer Research Program (through a Predoctoral Traineeship Award given to S.H.C.) W81XWH-10-1-0351. We would also like to thank A. Al-Zaki for TEM image acquisition. and C. Buckley and L. Murphy of the University of Pennsylvania School of Veterinary Medicine for ICP-MS measurements.

REFERENCES AND NOTES

1. Tennant, D. A.; Duran, R. V.; Gottlieb, E. Targeting Metabolic Transformation for Cancer Therapy. *Nat. Rev. Cancer* **2010**, *10*, 267–277.
2. Basu, S.; Alavi, A. Revolutionary Impact Of PET And PET-CT on the Day-to-Day Practice of Medicine and Its Great Potential for Improving Future Health Care. *Nucl. Med. Rev. Cent. East Eur.* **2009**, *12*, 1–13.
3. Nagrath, D.; Caneba, C.; Karedath, T.; Bellance, N. Metabolomics for Mitochondrial and Cancer Studies. *Biochim. Biophys. Acta* **2011**, *1807*, 650–663.
4. Ferreira, L. M. Cancer Metabolism: The Warburg Effect Today. *Exp. Mol. Pathol.* **2010**, *89*, 372–380.
5. Schornack, P. A.; Gillies, R. J. Contributions of Cell Metabolism and H+ Diffusion to the Acidic pH of Tumors. *Neoplasia* **2003**, *5*, 135–145.
6. Gillies, R. J.; Raghunand, N.; Garcia-Martin, M. L.; Gatenby, R. A. pH Imaging. A Review of pH Measurement Methods and Applications in Cancers. *IEEE Eng. Med. Biol. Mag.* **2004**, *23*, 57–64.
7. Gillies, R. J.; Raghunand, N.; Karczmar, G. S.; Bhujwalla, Z. M. MRI of the Tumor Microenvironment. *J. Magn. Reson. Imaging* **2002**, *16*, 430–50.
8. Stubbs, M.; Bhujwalla, Z. M.; Tozer, G. M.; Rodrigues, L. M.; Maxwell, R. J.; Morgan, R.; Howe, F. A.; Griffiths, J. R. An Assessment of ^{31}P MRS as a Method of Measuring pH in Rat Tumours. *NMR Biomed.* **1992**, *5*, 351–359.
9. Bhujwalla, Z. M.; McCoy, C. L.; Glickson, J. D.; Gillies, R. J.; Stubbs, M. Estimations of Intra- and Extracellular Volume and pH by ^{31}P Magnetic Resonance Spectroscopy: Effect of Therapy on RIF-1 Tumours. *Br. J. Cancer* **1998**, *78*, 606–611.
10. van Sluis, R.; Bhujwalla, Z. M.; Raghunand, N.; Ballesteros, P.; Alvarez, J.; Cerdan, S.; Galons, J. P.; Gillies, R. J. *In Vivo* Imaging of Extracellular pH Using ^{1}H MRSI. *Magn. Reson. Med.* **1999**, *41*, 743–750.
11. Aime, S.; Barge, A.; Delli Castelli, D.; Fedeli, F.; Mortillaro, A.; Nielsen, F. U.; Terreno, E. Paramagnetic Lanthanide(III) Complexes as pH-Sensitive Chemical Exchange Saturation Transfer (CEST) Contrast Agents for MRI Applications. *Magn. Reson. Med.* **2002**, *47*, 639–648.
12. Wu, Y.; Soesbe, T. C.; Kiefer, G. E.; Zhao, P.; Sherry, A. D. A Responsive Europium(III) Chelate That Provides a Direct Readout of pH by MRI. *J. Am. Chem. Soc.* **2010**, *132*, 14002–14003.
13. Thorek, D. L.; Chen, A. K.; Czupryna, J.; Tsourkas, A. Superparamagnetic Iron Oxide Nanoparticle Probes for Molecular Imaging. *Annu. Rev. Biomed. Eng.* **2006**, *34*, 23–38.
14. Deng, Z.; Zhen, Z.; Hu, X.; Wu, S.; Xu, Z.; Chu, P. K. Hollow Chitosan-Silica Nanospheres as pH-Sensitive Targeted Delivery Carriers in Breast Cancer Therapy. *Biomaterials* **2011**, *32*, 4976–4986.
15. Shenoy, D.; Little, S.; Langer, R.; Amiji, M. Poly(ethylene oxide)-Modified Poly(β-amino ester) Nanoparticles as a pH-Sensitive System for Tumor-Targeted Delivery of Hydrophobic Drugs. 1. *In Vitro* Evaluations. *Mol. Pharmaceutics* **2005**, *2*, 357–366.
16. Chawla, J. S.; Amiji, M. M. Biodegradable Poly(ε-Caprolactone) Nanoparticles for Tumor-Targeted Delivery of Tamoxifen. *Int. J. Pharm.* **2002**, *249*, 127–138.
17. Lee, E. S.; Na, K.; Bae, Y. H. Polymeric Micelle for Tumor pH and Folate-Mediated Targeting. *J. Controlled Release* **2003**, *91*, 103–113.
18. Paquet, C.; de Haan, H. W.; Leek, D. M.; Lin, H. Y.; Xiang, B.; Tian, G.; Kell, A.; Simard, B. Clusters of Superparamagnetic Iron Oxide Nanoparticles Encapsulated in a Hydrogel: A Particle Architecture Generating a Synergistic Enhancement of the T_2 Relaxation. *ACS Nano* **2011**, *5*, 3104–3112.
19. Li, Q.; Dunn, E. T.; Grandmaison, E. W.; Goosen, M. F. A. Applications and Properties of Chitosan. *J. Bioact. Compat. Polym.* **1992**, *7*, 370–397.
20. Enochs, W. S.; Harsh, G.; Hochberg, F.; Weissleder, R. Improved Delineation of Human Brain Tumors on MR Images Using a Long-Circulating, Superparamagnetic Iron Oxide Agent. *J. Magn. Reson. Imaging* **1999**, *9*, 228–232.
21. Moore, A.; Marecos, E.; Bogdanov, A., Jr.; Weissleder, R. Tumoral Distribution of Long-Circulating Dextran-Coated Iron Oxide Nanoparticles in a Rodent Model. *Radiology* **2000**, *214*, 568–574.
22. Zimmer, C.; Weissleder, R.; Poss, K.; Bogdanova, A.; Wright, S. C., Jr.; Enochs, W. S. MR Imaging of Phagocytosis in Experimental Gliomas. *Radiology* **1995**, *197*, 533–538.
23. Zimmer, C.; Wright, S. C., Jr.; Engelhardt, R. T.; Johnson, G. A.; Kramm, C.; Breakefield, X. O.; Weissleder, R. Tumor Cell Endocytosis Imaging Facilitates Delineation of fhe Glioma−Brain Interface. *Exp. Neurol.* **1997**, *143*, 61–69.
24. Frank, J. A.; Anderson, S. A.; Kalsih, H.; Jordan, E. K.; Lewis, B. K.; Yocum, G. T.; Arbab, A. S. Methods for Magnetically Labeling Stem and Other Cells for Detection by *In Vivo* Magnetic Resonance Imaging. *Cytotherapy* **2004**, *6*, 621–625.
25. Lewin, M.; Carlesso, N.; Tung, C. H.; Tang, X. W.; Cory, D.; Scadden, D. T.; Weissleder, R. Tat Peptide-Derivatized Magnetic Nanoparticles Allow *In Vivo* Tracking and Recovery of Progenitor Cells. *Nat. Biotechnol.* **2000**, *18*, 410–414.
26. Montet-Abou, K.; Montet, X.; Weissleder, R.; Josephson, L. Cell Internalization of Magnetic Nanoparticles Using Transfection Agents. *Mol. Imaging* **2007**, *6*, 1–9.
27. Thorek, D. L.; Tsourkas, A. Size, Charge and Concentration Dependent Uptake of Iron Oxide Particles by Non-phagocytic Cells. *Biomaterials* **2008**, *29*, 3583–3590.
28. Chouly, C.; Pouliquen, D.; Lucet, I.; Jeune, J. J.; Jallet, P. Development of Superparamagnetic Nanoparticles for MRI: Effect of Particle Size, Charge and Surface Nature on Biodistribution. *J. Microencapsulation* **1996**, *13*, 245–255.
29. Moghimi, S. M.; Davis, S. S. Innovations in Avoiding Particle Clearance from Blood by Kupffer Cells: Cause for Reflection. *Crit. Rev. Ther. Drug Carrier Syst.* **1994**, *11*, 31–59.
30. Moghimi, S. M.; Hunter, A. C.; Murray, J. C. Long-Circulating and Target-Specific Nanoparticles: Theory to Practice. *Pharmacol. Rev.* **2001**, *53*, 283–318.
31. Elias, D. R.; Cheng, Z.; Tsourkas, A. An Intein-Mediated Site-Specific Click Conjugation Strategy for Improved Tumor Targeting of Nanoparticle Systems. *Small* **2010**, *6*, 2460–2468.
32. Gallagher, F. A.; Kettunen, M. I.; Day, S. E.; Hu, D. E.; Ardenkjaer-Larsen, J. H.; Zandt, R.; Jensen, P. R.; Karlsson, M.; Golman, K.; Lerche, M. H.; Brindle, K. M. Magnetic Resonance Imaging of pH *in Vivo* Using Hyperpolarized ^{13}C-Labelled Bicarbonate. *Nature* **2008**, *453*, 940–943.
33. Andreev, O. A.; Dupuy, A. D.; Segala, M.; Sandugu, S.; Serra, D. A.; Chichester, C. O.; Engelman, D. M.; Reshetnyak, Y. K. Mechanism and Uses of a Membrane Peptide That Targets Tumors and Other Acidic Tissues *in Vivo*. *Proc. Natl. Acad. Sci. U.S.A.* **2007**, *104*, 7893–7898.
34. Andreev, O. A.; Engelman, D. M.; Reshetnyak, Y. K. Targeting Acidic Diseased Tissue: New Technology Based on Use of the pH (Low) Insertion Peptide (pHlip). *Chim Oggi* **2009**, *27*, 34–37.
35. Vavere, A. L.; Biddlecombe, G. B.; Spees, W. M.; Garbow, J. R.; Wijesinghe, D.; Andreev, O. A.; Engelman, D. M.; Reshetnyak, Y. K.; Lewis, J. S. A Novel Technology for the Imaging of Acidic Prostate Tumors by Positron Emission Tomography. *Cancer Res.* **2009**, *69*, 4510–4516.